Amor-Martin, A., Garcia-Castillo, L. E., & Garcia-Dooro, D. (2016). Second-Order Nédélec Curl-Conforming Prismatic Element for Computational Electromagnetics. *In IEEE Transactions on Antennas and Propagation, 64*(10), 4384–4395.

DOI:10.1109/tap.2016.2597640

Second-Order Nédélec Curl-Conforming Prismatic Element for Computational Electromagnetics

Adrian Amor-Martin, *Member, IEEE,* Luis Emilio Garcia-Castillo, *Member, IEEE,* and Daniel Garcia-Doñoro, *Member, IEEE,*

***Abstract*—A systematic approach to obtain mixed order curl-conforming basis functions for a triangular prism is presented; focus is made on the second-order case. Space of functions for the prism is given. Basis functions are obtained as dual basis with respect to properly discretized Nédélec degrees of freedom functionals acting on elements of the space. Thus, the linear independence of the basis functions is assured while the belonging of the basis to the *a-priori* given space of functions is guaranteed. Different strategies for the finite element assembly of the basis are discussed. Numerical results showing the verification procedure of the correctness of the implemented basis functions are given. Numerical results about sensibility with respect to quality of the elements of the mesh of the condition number of the basis obtained are also shown. Comparison with other representative sets of basis functions for prisms are included.**

***Index Terms*—Curl-conforming element, finite element calculations, Nédélec elements, triangular prismatic element.**

I. Introduction

Curl-conforming finite elements have been object of intensive research in the electromagnetic community during the nineties and early '00s providing stable discretization schemes for the electromagnetic field within the context of full wave vector formulations in electromagnetics. Two main types of curl-conforming elements may be distinguished depending on whether they are complete up to some order (in the polynomial sense) or not. The latter elements are called mixed order elements as they provide a mixed order approximation of the field while the approximation of the curl remains complete of one order less (as in their complete order counterpart) [1]. A detailed review of the literature in this subject up to 1997 may be found in [2]. It is worth noting later contributions: [3], [4], [5], [6], [7]. An intense research activity has been also carried out in the mathematical community identifying and solving a number of issues related with the application of finite elements to the full set of Maxwell Equations [8], being worth noting the sufficient condition for stability given by the commutativity of the de-Rham diagram [9].

Adrian Amor-Martin and Luis Emilio Garcia-Castillo are with the Department of Signal Theory and Communications, University Carlos III of Madrid, Leganés, Spain, e-mail: aamor@tsc.uc3m.es, luise@tsc.uc3m.es

Daniel Garcia-Doñoro is with the Department of Electrical and Computer Engineering, University of Macau, Macau, China, e-mail: dgdonoro@gmail.com

The research group to which the authors belong has developed its own family of higher order curl-conforming simplices of mixed order, [10], [11]. Specifically, curl-conforming tetrahedral elements are included in an in-house electromagnetic simulator named HOFEM (Higher Order Finite Element Method), [12]. HOFEM has demonstrated to be a reliable tool in the daily basis design tasks carried out by the antenna and microwave circuit researchers in the group. However, while tetrahedral shapes are very versatile for discretization of complex geometrical domains, mesh generation with tetrahedral elements can be very expensive computationally speaking, or simply not appropiate or efficient for a significant number of structures. That is the case of planar structures such as integrated circuits package designs, or planar microwave circuits and antennas, in which a volumetric mesh in terms of triangular prisms can be easily generated by extrusion of a two dimensional mesh based on triangles. Waveguide sections are also good candidates to be tessellated by extrusion with triangular prisms. The use of planar layers as coats to conformal surfaces may also be easily meshed with prisms; in this case the prisms are distorted (not parallel edges in the direction of "extrusion").

Despite its "apparent" simplicity, the number of implementations of curl-conforming triangular prisms appeared in the literature is considerably less than their tetrahedral counterparts. Geometrically speaking the triangular prism element is obtained by extrusion and hence, its basis function space naturally inherits a tensor product structure of the corresponding space of the two dimensional simplex (triangle) and the one dimensional space (segment). Mixed order property and stability conditions sum up to define the finite element space for the reference prism as it is explained later. In other words, given a function space for the triangular finite element, the space of basis functions for the reference prism is uniquely, and easily, defined. It is worth noting that, in contrast, basis functions for the triangular prism can not be directly defined in the general case as some sort of tensor product of the basis functions of the triangle and the nodal basis for the segment (even assuming appropriate constraints regarding polynomial orders of approximation in certain directions are satisfied for stability purposes).

Pioneering basis functions were given in [?], [13], [14]. Basis functions proposed in [15] may be considered an example of what was just mentioned above (functions given there fail to provide tangential continuity in the general case). A number of approaches to directly obtain higher order curl-conforming basis for the prisms, without a priori definition of the space,

have been proposed after then. Graglia et al., [16], propose functions for the prisms based on its popular well-known approach for simplices and hexahedra in affine coordinates of [17] overcoming the limitations of functions shown in [15]. Functions given in [18], [19] are obtained following the same methodology that in [20] for tetrahedral elements, which basically consists of imposing a number of constraints to a general expression for the basis functions in affine coordinates. The constraints are based on assumed properties of the space (e.g., the so called inclusion condition). There are as well constraints "inspired" by the definition of degrees of freedom of [1], [21]; however, no explicit expressions of the space or the use of degrees of freedom definitions are made in the obtainment of the basis functions. A different approach is the one followed in [22], [23] for the prism which is an extension of the one presented in [24]–[26] for triangle and tetrahedrons. The goal of this approach is to get orthogonal basis functions for time domain finite element formulations. Orthogonality is achieved by explicit orthogonalization formula and it is also based on numerical orthogonality in terms of a particular quadrature formula. However, it is not clear for the authors of the present paper what space of functions is being approximated; e.g., the dimension count of the space spanned by these basis functions does not agree with mixed or polynomial complete order prisms. It is worth noting that the tensor product structure of the prisms makes easy to build spectral versions of the prism in the extrusion direction. An example is the prism presented in [27]. **In addition to the above references to curl-conforming basis functions for the prism of interpolatory type, it is worth mentioning hierarchical basis for the prism as those of [?] which constitute the hierarchical version of those presented in [16]. Also, the family of higher order elements of variable order proposed in [28] contains prisms. Recently, [?] proposed a complete family that also includes prisms.**

In contrast, the systematic approach followed here to obtain mixed order curl-conforming basis functions for the prism is based on the *a priori* definition on a reference element of the space of basis functions and the obtainment of the basis functions as the dual basis with respect to a set of unisolvent degrees of freedom acting on the defined space, i.e., Ciarlet classic definition of finite element [29]. Basis functions in the real element are obtained by using the inverse of the jacobian matrix which assures curl-conformity and supports prismatic elements with curved boundaries through the concept of isoparametric element [30]. The above mentioned approach has demonstrated to be sound mathematically speaking and to provide stable and well conditioned basis for higher order simplices, [10], [11], [31].

Specifically, such an approach has a number of advantages. Firstly, the space of functions, which determines stability and convergence properties of the finite element method, is known. In several cases, properties of the space spanned by the basis functions are not clear, e.g., if it satisfies the so called inclusion condition for the gradients or not. Another example is the existence of Nédélec type spaces [32] with similar but not identical properties to the original Nédélec space; e.g., the basis functions or third order described in [3] belong to one of these Nédélec type spaces probably not deliberately. In the case of the prism, the space is easily defined using the tensor product, the curl-conforming space of the triangle and the nodal one-dimensional space of the segment.

Secondly, the *a priori* definition of a set of functionals acting on the space (degrees of freedom) makes operations as projection of a given function on the set of finite element basis functions (useful for Dirichlet boundary conditions, explicit forcing of continuity conditions when hybridizing with other codes, and so on) much easier. Unisolvency of the degrees of freedom must be proved; however, proof of unisolvency of Nédélec degrees of freedom was already given in [21].

To the authors' best knowledge, this is the first time the dual basis with respect to a concrete implementation of Nédélec's degrees of freedom are obtained for the prism and verified. **It is worth noting that although the basis functions of this paper are classified as interpolatory in contraposition to the group of hierarchical basis, they are not interpolatory strictly speaking. That is, basis functions are not designed to be non zero at one point and zero at all the others as it will be in Section II.** It is also worth noting that Nédélec definition of degrees of freedom of the prism, as it happens with other types of elements, is purely mathematical and not directly implementable. In this paper, a systematic methodology to "discretize" Nédélec degrees of freedom for the prism and to obtain a concrete set of basis functions is described. Methodologies for the assembly of the finite element prisms are also discussed. Approximability and convergence properties of the obtained prism finite element are verified in the context of the HOFEM simulator mentioned above. Specifically in this paper, the goal are the second-order basis functions as second order is the default polynomial order used by HOFEM.

The rest of the paper is organized as follows: in the Section II the element developed is presented and explained, with the definition of the basis function space, degrees of freedom and assembly; in the Section III some numerical results obtained are described and, finally, in the Section IV final conclusions of the communication are explained.

II. The triangular prismatic element

Following Ciarlet classic definition of finite element [29], the prism is defined by a geometrical domain, a space of functions and a set of degrees of freedom. The domain is a prism with a triangular base (see Figure 2). The basis functions space and the functionals acting as degrees of freedom are defined next.

A. Basis function space

The basis function space for the mixed-order reference prism of order k is constructed by taking tensor products of mixed-order space for the reference triangle $\boldsymbol{\mathcal{R}}_{\boldsymbol{k}}(T)$ with the space of one-dimensional polynomials on the reference segment $P_k(I)$:

$$\boldsymbol{\mathcal{P}}_{\boldsymbol{k}}^{\text{prism}} = (\boldsymbol{\mathcal{R}}_{\boldsymbol{k}}(T) \otimes P_k(I)) \times (\mathbf{P}_k(T) \otimes P_{k-1}(I)) \qquad (1)$$

$$\boldsymbol{\mathcal{R}_2}(T) = \left\{ \begin{array}{c} \alpha_1 + \alpha_2\xi + \alpha_3\eta + \gamma_1\eta^2 - \gamma_2\xi\eta \\ \beta_1 + \beta_2\xi + \beta_3\eta - \gamma_1\xi\eta + \gamma_2\xi^2 \end{array} \right\} \tag{2}$$

$$\boldsymbol{\mathcal{P}}_{\mathbf{2}}^{\text{prism}} \equiv \mathbf{N}_i (i = 1, ..., 36) = \left\{ \begin{array}{c} a_1^{(i)} + a_2^{(i)}\xi + a_3^{(i)}\eta + a_4^{(i)}\zeta + a_5^{(i)}\xi\zeta + a_6^{(i)}\eta\zeta + a_7^{(i)}\zeta^2 + a_8^{(i)}\xi\zeta^2 + ... \\ ... + a_9^{(i)}\eta\zeta^2 + C^{(i)}\eta^2 + D^{(i)}\xi\eta + E^{(i)}\eta^2\zeta + F^{(i)}\xi\eta\zeta + G^{(i)}\eta^2\zeta^2 + H^{(i)}\xi\eta\zeta^2 \\ \\ b_1^{(i)} + b_2^{(i)}\xi + b_3^{(i)}\eta + b_4^{(i)}\zeta + b_5^{(i)}\xi\zeta + b_6^{(i)}\eta\zeta + b_7^{(i)}\zeta^2 + b_8^{(i)}\xi\zeta^2 + ... \\ ... + b_9^{(i)}\eta\zeta^2 - C^{(i)}\xi\eta - D^{(i)}\xi^2 - E^{(i)}\xi\eta\zeta - F^{(i)}\xi^2\zeta - G^{(i)}\xi\eta\zeta^2 - H^{(i)}\xi^2\zeta^2 \\ \\ c_1^{(i)} + c_2^{(i)}\xi + c_3^{(i)}\eta + c_4^{(i)}\xi^2 + c_5^{(i)}\eta^2 + c_6^{(i)}\xi\eta + c_7^{(i)}\zeta + c_8^{(i)}\xi\zeta + ... \\ ... + c_9^{(i)}\eta\zeta + c_{10}^{(i)}\xi^2\zeta + c_{11}^{(i)}\eta^2\zeta + c_{12}^{(i)}\xi\eta\zeta \end{array} \right\} \tag{3}$$

where mixed-order curl conformity and satisfaction of commutativity of de-Rham diagram [9] are achieved by the properties of space $\boldsymbol{\mathcal{R}_k}(T)$ itself and by the use of one order less $(k-1)$ in the third dimensional direction of the prism. $\mathbf{P}_k(T)$ stands for the space of two-dimensional polynomials on the reference triangle. Note that boldface type fonts are used to denote vector magnitudes. In this paper, mixed-order space for the triangle $\boldsymbol{\mathcal{R}_k}(T)$ is precisely the Nédélec space [1] for the 2D simplex.

Text has been omitted here, including equation (2) and (3) of the original submitted version. Table I of the original version is also omitted.

The dimension of the polynomial spaces involved in the prism space definition of (1) are 9, 36 and 90 for the first, second and third order cases, respectively. In the following the focus will be set on the second-order functions. Explicit expressions of elements of space $\boldsymbol{\mathcal{R}_2}(T)$ are given in (2) (see [10], [2]). Thus, the corresponding space $\boldsymbol{\mathcal{P}}_{\mathbf{2}}^{\text{prism}}$ for the prism may be given as in (3).

It is worth to note that the basis function space for the prism (3) is not *isotropic*. If we interchange, for instance, ξ and ζ coordinates the resulting space does not have an equivalent expression to (3) in contrast to tetrahedral Nédélec space in which we can interchange any three of the coordinates. This fact will have to be taken into account when interpreting some of the numerical results shown later.

Elements of the spaces are determined by coefficients a_1, a_2, C, and so on, of (3). Specifically, the basis functions $\mathbf{N}_i$ of the corresponding space are obtained as dual basis with respect to a set of $g_i(\mathbf{u})$ functionals (degrees of freedom in FEM terminology). That is, for the second order case, $\mathbf{N}_i, i = 1 \ldots 36$ should satisfy the following 36 equalities compactly expressed as:

$$g_i(\mathbf{N}_j) = \delta_{ij}, \quad i, j = 1 \ldots 36 \tag{4}$$

where δ_{ij} refers to Kronecker delta.

Functionals degrees of freedom g_i are defined in the following.

B. Degrees of freedom

The definition of the types of functionals which are used as the $g_i(\mathbf{u})$ degrees of freedom of the second order prismatic element is as follows [21, Definition 8], where $\mathbf{u}$ stands for elements of $\boldsymbol{\mathcal{P}}_{\mathbf{2}}^{\text{prism}}$ (in practice, the electromagnetic field). The spacial locations **to which associate** these degrees of freedom in the reference prism are shown in the Figure 2.

1) Degrees of freedom associated to edges, defined as:
$$g(\mathbf{u}) = \int_e (\mathbf{u} \cdot \hat{\boldsymbol{\tau}}) q \, dl, \forall q \in P_1(e) \tag{5}$$
where e stands for *edge*, $\hat{\boldsymbol{\tau}}$ is the unit vector tangent to the considered edge, and $P_1(e)$ is the space of scalar first order polynomials in the corresponding edge local coordinate.
2) Degrees of freedom associated to triangular faces, defined as:
$$g(\mathbf{u}) = \int_{f_t} (\mathbf{u} \times \hat{\mathbf{n}}) \cdot \mathbf{q} \, ds, \forall \mathbf{q} \in \mathbf{P}_0(f_t) \tag{6}$$
where f_t stands for *triangular face*, $\hat{\mathbf{n}}$ is the outward unit normal vector to the considered face, and $\mathbf{P}_0(f_t)$ is the space of two component vector zero order polynomials in the corresponding two local coordinates of the triangular face.
3) Degrees of freedom associated to quadrilateral faces, defined as:
$$g(\mathbf{u}) = \int_{f_q} (\hat{\mathbf{n}} \times \mathbf{u}) \cdot \mathbf{q} \, ds \quad \forall \mathbf{q} = (q_1, q_2); q_1 \in \mathcal{Q}_{0,1}; q_2 \in \mathcal{Q}_{1,0} \tag{7}$$
where $\hat{\mathbf{n}}$ is again the outward unit normal vector to the considered quadrilateral face f_q. Space $\mathcal{Q}_{l,m}$ is the space of scalar vector polynomials in the corresponding local variables (x_1, x_2) of the quadrilateral face such as the maximum degree is l in x_1 and m in x_2. Note that typically (but not necessarily), either x_1 or x_2, is chosen as the extrusion direction of the prism. Note again that the approximation is of one order less in the direction of the component considered.
4) Degrees of freedom associated to the volume, defined as
$$g(\mathbf{u}) = \int_v \mathbf{u} \cdot \mathbf{q} \, dV, \forall \mathbf{q} \in \mathbf{P}_0(f_t) \tag{8}$$
where vector polynomial $\mathbf{q}$ are, as in the case of degrees of freedom associated to triangular faces, two component vector polynomials in the corresponding two "horizontal" local coordinates. Thus, the same notation as in triangular face degrees of freedom is used for space of $\mathbf{q}$ polyno-

mials here.

It is worth noting that, in addition to volume degrees of freedom as those of (8), another type of volume degree of freedom appears for prism of order three and above.

Each one of the degrees of freedom defined above is associated to a basis function (see (4)). Thus, basis functions are naturally associated to edges, faces and volume of the prism. The definition of the degrees of freedom associated to finite element boundaries (edges and faces) only involves tangential components. Thus, it eases to get tangential continuity (continuity in the curl sense) between finite elements since only basis functions associated to a given part of the prism boundary will give non-null trace (in the tangential sense) on that considered part of the boundary. For the same reason, basis functions associated to the prism volume are not involved in the finite element assembly as they provide null trace on the prism boundary. Note that degrees of freedom corresponding to edges are defined as in Nédélec tetrahedra and hexahedra and that degrees of freedom associated to triangular and quadrilateral faces are defined in the same way as in Nédélec tetrahedra and hexahedra faces, respectively. **That makes possible the support of meshes containing tetrahedra and hexahedra.**

C. Discretization of degrees of freedom

The definition of degrees of freedom as above can be used to prove unisolvency; i.e., to ensure that basis functions obtained from (4) are linearly independent. However, they can not be implemented in order to obtain specific basis functions to be used in a finite element code. For that purpose, the degrees of freedom must be somehow "discretized". The discretization is performed by means of the choice of a basis for each one of the polynomial spaces appearing in the definition of the degrees of freedom. Thus, definition of degrees of freedom is made in terms of momentums (of different order) over the adequate components of the vector unknown $\mathbf{u}$.

1) Edges: Let us consider the degrees of freedom associated to edges first. A basis for $P_1(e)$, i.e., the space of first order scalar polynomials with the local edge coordinate as variable has to be chosen. As an example, consider the edge going from vertex #1 to vertex #2 of reference element shown in Figure 2. For that edge, local coordinate is ξ. Thus, a possible basis for $P_1(e)$ might be $q_1 = 1$, $q_2 = \xi$. However, as the goal is to obtain interpolatory basis functions, it is better to use an interpolatory basis for $P_1(e)$. The advantages of choosing interpolatory basis for q are a better conditioning of the resulting basis (based on the experience of the authors with tetrahedra elements) and an easier implementation of the finite element assembly. The latter is due to the natural association of degrees of freedom (equivalently basis functions) to nodes placed in certain points/parts of the edge (or prism in general). Thus, information about connectivity of the finite element shape functions of the mesh can be gathered with conventional FEM mesh software (maybe with some minor tweaking) in terms of nodes. Specifically, Lagrange polynomials are chosen in this paper and hence, $q_1 = 1 - \xi$, $q_2 = \xi$. Thus, the first degree of freedom of the considered edge should be associated to vertex #1 and the second one to vertex #2. They are the degrees of freedom 1 and 2 in Figure 2. Actually, the degrees of freedom associated to edges are not drawn at the edge vertices but close to them on the edge. Finally, note that with other edges the local coordinate/parametrization would be different; e.g., for the edge going from vertex #2 to vertex #3 local coordinate e is equal to $(1 - \xi + \eta)/2$ leading to $q_1 = 1 - e = \xi$, $q_2 = e = \eta$ since $1 - \xi = \eta$ over the edge.

2) Triangular faces: Analogously, a basis for the vector $\mathbf{q}$ has to be chosen for face and volume degrees of freedom. Discretization of degrees of freedom associated to the the two triangular faces of the prism (6) involves space $\mathbf{P}_0(f_t)$, i.e., space of constant vectors on the plane ξ, η. Thus, we simply have to choose two directions on the plane ξ, η; denoted by unit vectors $\hat{\boldsymbol{\alpha}}$ and $\hat{\boldsymbol{\beta}}$. A possible choice is $\hat{\boldsymbol{\alpha}} = \hat{\boldsymbol{\xi}}$, $\hat{\boldsymbol{\beta}} = \hat{\boldsymbol{\eta}}$ which corresponds to degrees of freedom 19, 20 of lower triangular face of the prism and degrees of freedom 21, 22 of upper triangular face (see Figure 2). Note that two orthogonal directions have been chosen, which is relevant as it will be explained in Section II-E.

3) Quadrilateral faces: Discretization of degrees of freedom associated to the two quadrilateral faces of the prism (7) also involves the choice of two directions on the plane corresponding to the quadrilateral face, e.g., the plane $\xi - \zeta$ for face of vertices #1-#2-#5-#4. Let us denote them by their unit vectors $\hat{\boldsymbol{\alpha}}$ and $\hat{\boldsymbol{\beta}}$. Let us consider we choose $\hat{\boldsymbol{\alpha}} = \hat{\boldsymbol{\xi}}$ and $\hat{\boldsymbol{\beta}} = \hat{\boldsymbol{\zeta}}$ on the mentioned face. The choice of scalar polynomials q is different to the case of the triangular faces because q is no longer a constant and specially because the "one order less" property have to be satisfied by $\mathbf{q}$, i.e., $\mathbf{q} \in \mathcal{Q}_{0,1} \times \mathcal{Q}_{1,0}$. Thus, a reasonable choice for a basis of $\mathbf{q}$ space might be $\mathbf{q}_1 = (1 - \zeta)\hat{\boldsymbol{\xi}}$, $\mathbf{q}_2 = \zeta\hat{\boldsymbol{\xi}}$, $\mathbf{q}_3 = (1 - \xi)\hat{\boldsymbol{\zeta}}$, $\mathbf{q}_4 = \xi\hat{\boldsymbol{\zeta}}$ in this example (see association of degrees of freedom 23–26 to different zones and directions of the face in Figure 2 with $\mathbf{q}_1$, $\mathbf{q}_2$, $\mathbf{q}_3$ and $\mathbf{q}_4$ as degrees 23, 24, 25 and 26, respectively).

4) Interior: The space of $\mathbf{q}$ for degrees of freedom associated to volume (8) is $\mathbf{P}_0(f_t)$, i.e., the same than the one of triangular faces. Thus, the choice for $\mathbf{q}$ may be made as in the degrees of freedom associated to the triangular face. See degrees of freedom 35, 36 in Figure 2.

D. Dual basis

It is worth noting that the same methodology above described for discretization of Nédélec degrees of freedom of second order can be applied for higher orders (e.g., see [11] for third-order tetrahedron).

As it was already mentioned, once the degrees of freedom have been discretized, i.e., basis for spaces of scalars q and vector $\mathbf{q}$ polynomials involved have been selected, the basis functions are obtained as dual basis with respect to discretized degrees of freedom functionals. That means each one of the 36 basis functions $\mathbf{N}_i$ is obtained by imposing the corresponding 36 relations given by (4). Thus, each $\mathbf{N}_i$ is naturally associated to a degree of freedom g_i. In practice, forcing (4) implies solving a matrix system of equations of dimension 36 with 36 right-hand sides in which the unknowns are the coefficients a_1, a_2, $C \ldots$ of (3). Thus, $a_1^{(1)}$, $a_2^{(1)}$, $C^{(1)}$ $\ldots$ would be obtained

TABLE I: Choice of scalars q and vectors $\mathbf{q}$ used in the obtention of coefficients of Table II for each degree of freedom (DOF). Scalar q is used for DOF from 1 to 18, and a vectorial $\mathbf{q}$ is taken for DOF from 19 to 36.

DOF	q or $\mathbf{q}$	DOF	$\mathbf{q}$
$1, 7$	$1-\xi$	24	$\zeta \cdot \hat{\boldsymbol{\xi}}$
$2, 8$	ξ	25	$(1-\xi) \cdot \hat{\boldsymbol{\zeta}}$
$3, 9$	ξ	26	$\xi \cdot \hat{\boldsymbol{\zeta}}$
$4, 10$	η	27	$(1-\zeta) \cdot (-\hat{\boldsymbol{\xi}} + \hat{\boldsymbol{\eta}})/\sqrt{2}$
$5, 11$	η	28	$\zeta \cdot (-\hat{\boldsymbol{\xi}} + \hat{\boldsymbol{\eta}})/\sqrt{2}$
$6, 12$	$1-\eta$	29	$\xi \cdot \hat{\boldsymbol{\zeta}}$
$13, 15, 17$	$1-\zeta$	30	$\eta \cdot \hat{\boldsymbol{\zeta}}$
$14, 16, 18$	ζ	31	$(1-\zeta) \cdot \hat{\boldsymbol{\eta}}$
$19, 21, 35$	$\hat{\boldsymbol{\xi}}$	32	$\zeta \cdot \hat{\boldsymbol{\eta}}$
$20, 22, 36$	$\hat{\boldsymbol{\eta}}$	33	$\eta \cdot \hat{\boldsymbol{\zeta}}$
23	$(1-\zeta) \cdot \hat{\boldsymbol{\xi}}$	34	$(1-\eta) \cdot \hat{\boldsymbol{\zeta}}$

for the first basis function $\mathbf{N}_1$. Analogously, $\mathbf{N}_2$, $\mathbf{N}_3$, and so on. **Pseudocode of the procedure to get the coefficients is shown in Figure 1.** Specifically, considering basis for q, $\mathbf{q}$ shown in Table I, coefficients given in Table II are obtained. **Thus, it is clear basis functions so obtained are not interpolatory strictly speaking. Actually, there are no interpolatory points involved in the definition of either the basis or the degrees of freedom. The interpolatory character and the association of basis functions to certain regions of the edges, faces and interior is indirect through the interpolatory character of the polynomials used as basis for the polynomial spaces involved in the definition of the functional degrees of freedom as weighted momentums.**

The procedure just described to obtain the basis functions can be applied to any prism. However, there is a number of advantages in the use of the concept of reference finite element. Thus, basis functions are obtained in the reference element (shown in Figure 2) and transformed into the real element (actual element of the mesh) by using the following transformation:

$$\mathbf{u} = [\mathbf{J}]^{-1}\mathbf{u}^r \tag{9}$$

where $[\mathbf{J}]$ stands for the Jacobian matrix of the geometric transformation, $\mathbf{u}^r$ denotes a vector in the reference element and $\mathbf{u}$ the mapped vector in the real element.

Note that (9) transforms vectors as the gradients being the appropriate transformation for curl-conforming elements. It is important to know how (9) affects to vector magnitudes involved in the definition of degrees of freedom since it is relevant for the assembly procedure. This question is addressed next in Section II-E.

E. Assembly

As it has been shown in the previous section, each degree of freedom, and hence its corresponding basis function may be associated to an entity (edge, face, or volume) of the prism. Within its entity a degree of freedom is associated to a "zone" (where the associated node is placed) of that edge, face and

Require: $g_e(\text{edge\_number}, \mathbf{u}, q) \leftarrow$ evaluation of (5)
Require: $g_{f_t}(\text{face}, \mathbf{u}, \mathbf{q}) \leftarrow$ evaluation of (6)
Require: $g_{f_q}(\text{face}, \mathbf{u}, \mathbf{q}) \leftarrow$ evaluation of (7)
Require: $g_v(\mathbf{u}, \mathbf{q}) \leftarrow$ evaluation of (8)

Input: q_e ▷ Scalar polynomials defined on segment (edge)
Input: $\mathbf{q}$ ▷ Vector polynomials defined on plane (face)
Output: **coef** ▷ Coefficient matrix that defines basis functions

1: **procedure** NI_COEF(q,$\mathbf{q}$,**coef**)
Vector monomials $\mathbf{u}_i$ associated to coefficients **coef**
coef(:,i) =$[a_1, \ldots, a_9, b_1, \ldots, b_9, C, \ldots, H, c_1, \ldots, c_{12}]$
2: $\mathbf{u}_1 = (1, 0, 0)$ ▷ Vector monomial associated to a_1
⋮
3: $\mathbf{u}_{10} = (0, 1, 0)$ ▷ Vector monomial associated to b_1
⋮
4: $\mathbf{u}_{19} = (\eta^2, -\xi\eta, 0)$ ▷ Vector monomial linked to C
⋮
5: $\mathbf{u}_{36} = (0, 0, \xi\eta\zeta)$ ▷ Vector monomial linked to c_{12}

Definition of degrees of freedom functionals
6: $g_1(\mathbf{u}) \leftarrow g_e(1, \mathbf{u}, q_1)$ ▷ First dof of first edge
7: $g_2(\mathbf{u}) \leftarrow g_e(1, \mathbf{u}, q_2)$ ▷ Second dof of first edge
⋮
8: $g_{18}(\mathbf{u}) \leftarrow g_e(9, \mathbf{u}, q_{18})$ ▷ Second dof of ninth edge
9: $g_{19}(\mathbf{u}) \leftarrow g_{f_t}(\text{bottom\_face}, \mathbf{u}, \mathbf{q}_{19})$ ▷ First dof of bottom triangular face
⋮
10: $g_{22}(\mathbf{u}) \leftarrow g_{f_t}(\text{upper\_face}, \mathbf{u}, \mathbf{q}_{22})$ ▷ Second dof of upper triangular face
11: $g_{23}(\mathbf{u}) \leftarrow g_{f_q}(\text{face } \xi - \zeta, \mathbf{u}, \mathbf{q}_{23})$ ▷ First dof of face $\xi - \zeta$ (vertices #1-#2-#5-#4)
⋮
12: $g_{35}(\mathbf{u}) \leftarrow g_v(\mathbf{u}, \mathbf{q}_{35})$ ▷ First dof of volume
13: $g_{36}(\mathbf{u}) \leftarrow g_v(\mathbf{u}, \mathbf{q}_{36})$ ▷ Second dof of volume

14: Coefficients **coef** obtained by the imposition of (4): $\mathbf{A} \times \mathbf{coef} = \mathbf{b}$
15: $A(i, j) \leftarrow g_i(\mathbf{u}_j)$ ▷ Filling of matrix $\mathbf{A}$
16: $\mathbf{b} \leftarrow \mathbb{I}_{36}$ ▷ RHS is identity matrix
17: **coef**$\leftarrow$ solve$(\mathbf{A}, \mathbf{b})$
18: **end procedure**

Fig. 1: **Pseudocode to obtain the values of the coefficients of expression (3) that define the basis functions. Coefficients are stored in matrix variable *coef*. Each column of matrix *coef* stores the coefficients of one basis function in the following order: $a_1, \ldots, a_9, b_1, \ldots, b_9, C, \ldots, H, c_1, \ldots, c_{12}$. The value of scalar $q_i, i = 1, \ldots, 18$ and $\mathbf{q}_j$, $j = 19, \ldots, 36$ are shown in Table I.**

TABLE II: Coefficients of expression (3) corresponding to basis functions in the reference element and choices of scalars q and vectors $\mathbf{q}$ shown in Table I.

a_1	a_2	a_3	a_4	a_5	a_6	a_7	a_8	a_9	b_1	b_2	b_3	b_4	b_5	b_6	b_7	b_8	b_9
4	−6	−12	−16	24	48	12	−18	−36	0	6	0	0	−24	0	0	18	0
−2	6	2	8	−24	−8	−6	18	6	0	−4	0	0	16	0	0	−12	0
0	0	2	0	0	−8	0	0	6	0	−4	0	0	16	0	0	−12	0
0	0	4	0	0	−16	0	0	12	0	−2	0	0	8	0	0	−6	0
0	0	4	0	0	−16	0	0	12	2	−2	−6	−8	8	24	6	−6	−18
0	0	−6	0	0	24	0	0	−18	−4	12	6	16	−48	−24	−12	36	18
0	0	0	−8	12	24	12	−18	−36	0	0	0	0	−12	0	0	18	0
0	0	0	4	−12	−4	−6	18	6	0	0	0	0	8	0	0	−12	0
0	0	0	0	0	−4	0	0	6	0	0	0	0	8	0	0	−12	0
0	0	0	0	0	−8	0	0	12	0	0	0	0	4	0	0	−6	0
0	0	0	0	0	−8	0	0	12	0	0	0	−4	4	12	6	−6	−18
0	0	0	0	0	12	0	0	−18	0	0	0	8	−24	−12	−12	36	18
0	0	0	0	0	0	0	0	0	0	0	0	0	0	0	0	0	0
0	0	0	0	0	0	0	0	0	0	0	0	0	0	0	0	0	0
0	0	0	0	0	0	0	0	0	0	0	0	0	0	0	0	0	0
0	0	0	0	0	0	0	0	0	0	0	0	0	0	0	0	0	0
0	0	0	0	0	0	0	0	0	0	0	0	0	0	0	0	0	0
0	0	0	0	0	0	0	0	0	0	0	0	0	0	0	0	0	0
0	0	−16	0	0	64	0	0	−48	0	8	0	0	−32	0	0	24	0
0	0	−8	0	0	32	0	0	−24	0	16	0	0	−64	0	0	48	0
0	0	0	0	0	−32	0	0	48	0	0	0	0	16	0	0	−24	0
0	0	0	0	0	−16	0	0	24	0	0	0	0	32	0	0	−48	0
0	0	0	−24	36	72	24	−36	−72	0	0	0	0	−36	0	0	36	0
0	0	0	12	−36	−12	−12	36	12	0	0	0	0	24	0	0	−24	0
0	0	0	0	0	0	0	0	0	0	0	0	0	0	0	0	0	0
0	0	0	0	0	0	0	0	0	0	0	0	0	0	0	0	0	0
0	0	0	0	0	−12	0	0	12	0	0	0	0	24	0	0	−24	0
0	0	0	0	0	−24	0	0	24	0	0	0	0	12	0	0	−12	0
0	0	0	0	0	0	0	0	0	0	0	0	0	0	0	0	0	0
0	0	0	0	0	0	0	0	0	0	0	0	0	0	0	0	0	0
0	0	0	0	0	−24	0	0	24	0	0	0	−12	12	36	12	−12	−36
0	0	0	0	0	36	0	0	−36	0	0	0	24	−72	−36	−24	72	36
0	0	0	0	0	0	0	0	0	0	0	0	0	0	0	0	0	0
0	0	0	0	0	0	0	0	0	0	0	0	0	0	0	0	0	0
0	0	0	0	0	−96	0	0	96	0	0	0	0	48	0	0	−48	0
0	0	0	0	0	−48	0	0	48	0	0	0	0	96	0	0	−96	0

C	D	E	F	G	H	c_1	c_2	c_3	c_4	c_5	c_6	c_7	c_8	c_9	c_{10}	c_{11}	c_{12}
8	8	−32	−32	24	24	0	0	0	0	0	0	0	0	0	0	0	0
0	−8	0	32	0	−24	0	0	0	0	0	0	0	0	0	0	0	0
0	−8	0	32	0	−24	0	0	0	0	0	0	0	0	0	0	0	0
−8	0	32	0	−24	0	0	0	0	0	0	0	0	0	0	0	0	0
−8	0	32	0	−24	0	0	0	0	0	0	0	0	0	0	0	0	0
8	8	−32	−32	24	24	0	0	0	0	0	0	0	0	0	0	0	0
0	0	−16	−16	24	24	0	0	0	0	0	0	0	0	0	0	0	0
0	0	0	16	0	−24	0	0	0	0	0	0	0	0	0	0	0	0
0	0	0	16	0	−24	0	0	0	0	0	0	0	0	0	0	0	0
0	0	16	0	−24	0	0	0	0	0	0	0	0	0	0	0	0	0
0	0	16	0	−24	0	0	0	0	0	0	0	0	0	0	0	0	0
0	0	−16	−16	24	24	0	0	0	0	0	0	0	0	0	0	0	0
0	0	0	0	0	0	4	−16	−16	12	12	24	−6	24	24	−18	−18	−36
0	0	0	0	0	0	−2	8	8	−6	−6	−12	6	−24	−24	18	18	36
0	0	0	0	0	0	0	−8	0	12	0	0	0	12	0	−18	0	0
0	0	0	0	0	0	0	4	0	−6	0	0	0	−12	0	18	0	0
0	0	0	0	0	0	0	0	−8	0	12	0	0	0	12	0	−18	0
0	0	0	0	0	0	0	0	4	0	−6	0	0	0	−12	0	18	0
16	8	−64	−32	48	24	0	0	0	0	0	0	0	0	0	0	0	0
8	16	−32	−64	24	48	0	0	0	0	0	0	0	0	0	0	0	0
0	0	32	16	−48	−24	0	0	0	0	0	0	0	0	0	0	0	0
0	0	16	32	−24	−48	0	0	0	0	0	0	0	0	0	0	0	0
0	0	−48	−48	48	48	0	0	0	0	0	0	0	0	0	0	0	0
0	0	0	48	0	−48	0	0	0	0	0	0	0	0	0	0	0	0
0	0	0	0	0	0	0	24	0	−24	0	−24	0	−36	0	36	0	36
0	0	0	0	0	0	0	−12	0	12	0	12	0	36	0	−36	0	−36
0	0	0	48	0	−48	0	0	0	0	0	0	0	0	0	0	0	0
0	0	48	0	−48	0	0	0	0	0	0	0	0	0	0	0	0	0
0	0	0	0	0	0	0	0	0	0	0	$12\sqrt{2}$	0	0	0	0	0	$-36/\sqrt{2}$
0	0	0	0	0	0	0	0	0	0	0	$-12/\sqrt{2}$	0	0	0	0	0	$36/\sqrt{2}$
0	0	48	0	−48	0	0	0	0	0	0	0	0	0	0	0	0	0
0	0	−48	−48	48	48	0	0	0	0	0	0	0	0	0	0	0	0
0	0	0	0	0	0	0	0	−24	0	24	24	0	0	36	0	−36	−36
0	0	0	0	0	0	0	0	12	0	−12	−12	0	0	−36	0	36	36
0	0	96	48	−96	−48	0	0	0	0	0	0	0	0	0	0	0	0
0	0	48	96	−48	−96	0	0	0	0	0	0	0	0	0	0	0	0

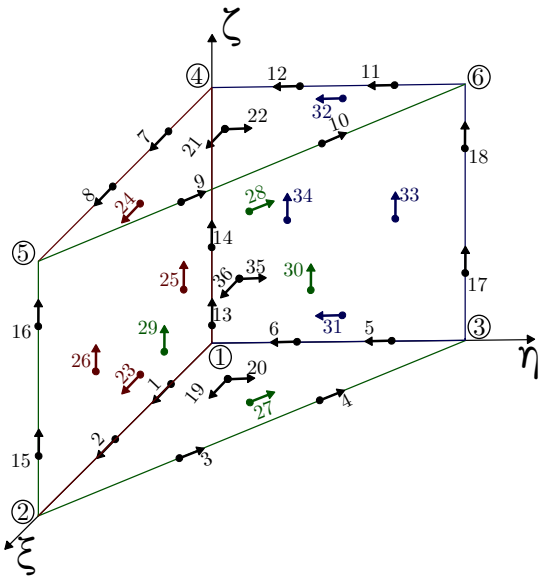

Fig. 2: Numeration of degrees of freedom **in the reference** prism of second order in which the length of the edges corresponding to the axes is 1.

volume. Furthermore, a degree of freedom also has a vector "direction" as it is illustrated in Figure 2 using arrows.

The procedure of assembly of two finite element matrices is based on making equal the values of the pairs of degrees of freedom of the two elements of the mesh that "coincide" when they are put together as it can be seen in Figure 3. In the Figure 3a it can be seen that the equalities in the face $g_{23}^{(1)} = g_{24}^{(2)}$, $g_{24}^{(1)} = g_{23}^{(2)}$, $g_{25}^{(1)} = -g_{25}^{(2)}$ and $g_{26}^{(1)} = -g_{26}^{(2)}$ have to be defined. A similar criteria must be followed with the degrees of freedom associated to the edges. **These differences in the senses can be symply managed through the definition of a global *sign* function similarly to the one defined in [10] for the tetrahedra (see also [2]) that multiplies unit vectors $\hat{\boldsymbol{\tau}}$ and $\hat{\mathbf{n}}$.**

Text has been omitted here. Text omitted included the lengthy explanation of the issue of the different local signs of the unit vectors $\hat{\boldsymbol{\tau}}$ and $\hat{\mathbf{n}}$. Emphasis on the case of vectors $\mathbf{q}$ polynomial has been kept.

The case of vectors $\mathbf{q}$ is more involved. Let us choose some arbitrary $\mathbf{q}$ in the reference element obtaining the basis functions on the reference element and then transformed trough (9) for two different neighbor elements of the mesh. In that case, the traces (in the tangential sense) of basis functions of one element and its neighbor on a shared face of the mesh will not be equal. In other words, (curl) conformity of the finite element approximation will be lost. Two strategies to deal with this issue are proposed (and implemented in HOFEM code).

1) Assembly vq*:* One strategy, which will denote as *vq*, is to choose unique sets of $\mathbf{q}$ on each face of the mesh and transform them to the reference element using (9) for each one of the two finite elements of the elements sharing that face. Vector $\mathbf{q}$ transformed to the reference element will be denoted by $\mathbf{q}^r$. In general, different $\mathbf{q}^r$ will be obtained for one element and its neighbor. Thus, coefficients (as those of Table II) for the basis functions need to be recalculated for each element. Note however that the choice of $\mathbf{q}$ on one face of the element only affects to the coefficients associated to the basis functions of the face. In the code, this strategy is parallelly implemented by a finite element initialization routine that loops over elements of the mesh and calculates coefficients of basis functions for each element. Thus, curl-conformity is preserved while arbitrary directions for pairs of $\mathbf{q}$ on each (triangular or quadrilateral) face can be chosen. Specifically, orthogonal directions for $\mathbf{q}$ (denoted as $\hat{\boldsymbol{\alpha}}$ and $\hat{\boldsymbol{\beta}}$ previously in Section II-B) may be chosen with a very positive impact in the conditioning of the resulting finite element matrices. See some numerical results in Section III.

2) Assembly vc*:* Another strategy, which will denote as *vc*, is to choose pairs of $\mathbf{q}$ on each face of the mesh in such a way that each $\mathbf{q}$ is parallel (directions $\hat{\boldsymbol{\alpha}}$ and $\hat{\boldsymbol{\beta}}$) to the edges of the face. It can be demonstrated that with such a choice of $\mathbf{q}$ vectors, transformation (9) yields to $\mathbf{q}^r$ with identical components parallel to the edges of the face, i.e., same edge trace on both neighbor elements sharing a common face of the mesh. In other words, pairs of $\mathbf{q}^r$ in the reference element can be chosen so the coefficients are obtained once in the reference element (e.g., those on Table I), being valid for all elements of the mesh. This strategy is implemented by a simple finite element initialization routine that is executed only once. Actually, this initialization routine computes a super-set of basis functions coefficients corresponding to the different pairs of directions that can be chosen on a face in the general case: e.g. directions parallel to edges 1-2, edges 2-3 or edges 3-1 for the triangular face, and parallel to edges 1-2, edges 2-3, edges 3-4, or edges 4-1 for the quadrilateral face. Later, the routine that performs the numerical integration of the entries of the finite element matrices selects a pair of edge directions for each face of the mesh based on some global criterion (typically, to select $\hat{\boldsymbol{\alpha}}$ and $\hat{\boldsymbol{\beta}}$ the closest to the orthogonal case as possible). Thus, curl-conformity is preserved without the need of computing different coefficients for different elements of the mesh. On the other hand, the behavior of strategy *vc* in terms of condition number with severe elongated elements is not as good as with strategy *vq* described previously as it will be explained in Section III. This is because the directions $\hat{\boldsymbol{\alpha}}$ and $\hat{\boldsymbol{\beta}}$ may be far from orthogonal as they have to be necessarily chosen parallel to the edges of the face.

Finally, it is worth noting to emphasize that $\mathbf{q}$ are, in general, polynomials. That is, vectors $\mathbf{q}$ are determined not only by its directions but also by their scalar polynomials q. For the particular case of second order prism which is the one under study here vectors $\mathbf{q}$ are constant for degrees of freedom on the triangular faces and the assembly has to take care of choosing the right direction ($\hat{\boldsymbol{\alpha}}$ or $\hat{\boldsymbol{\beta}}$) when processing each neighbor element sharing that face. In the case of the quadrilateral faces, not only directions ($\hat{\boldsymbol{\alpha}}$ or $\hat{\boldsymbol{\beta}}$) have to match between elements but also the scalar polynomial q associated. As an example, in Figure 3a the degree of freedom associated to $\mathbf{q}_{24}^{(1)}$ has to match to $\mathbf{q}_{23}^{(2)}$ instead of $\mathbf{q}_{24}^{(2)}$ although they have the same direction. This is implemented in HOFEM code via a local parametrization of arbitrary directions.

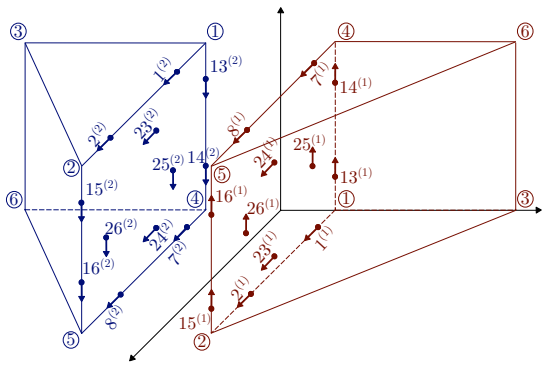

(a)

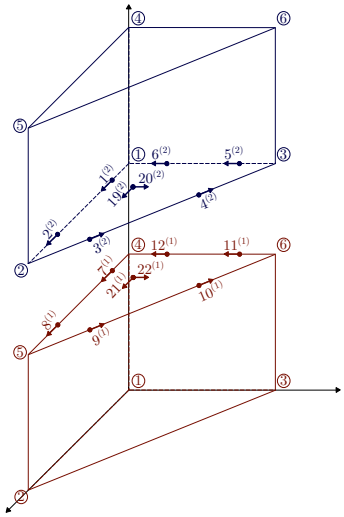

(b)

Fig. 3: Two cases of assembly between two prisms: (a) when a quadrilateral face is shared, and (b) when a triangular face is shared. The circumferences show the vertices numeration, while the superscript $^{(i)}$ present in the degrees of freedom stands for the number of the element.

III. Numerical Results

Several numerical results follow, where the main goal is the verification of the correctness of the basis functions implemented. **Results about conditioning of the basis are also presented in comparison with other representative sets of basis functions appeared in the literature.**

The verification is performed by using the Method of Manufactured Solutions (MMS) [**?**], [33], [34]. This method consists of "manufacturing" an exact solution to some partial differential equation by solving the problem backwards. If an equation of the type $D\boldsymbol{u} = \boldsymbol{f}$ —where D is the differential operator, $\boldsymbol{u}$ is the solution and $\boldsymbol{f}$ is the source term— has to be solved, $\boldsymbol{u}$ is manufactured and then the equation is applied to find $\boldsymbol{f}$.

In our case, the second order prismatic finite element presented here has been implemented in our own finite element code HOFEM [12], [35] which originally works with tetrahedral elements. HOFEM makes use of a double curl vector wave equation in terms of either the electric field or the magnetic field (see correspondences in Table III),

TABLE III: Formulation magnitudes and parameters. In the general case, ϵ_r and μ_r are represented in HOFEM by matrices but for simplicity they are denoted here as scalar magnitudes.

	$\mathbf{V}$	f_r	g_r	h	Γ_{D}	Γ_{N}
Form. $\mathbf{E}$	$\mathbf{E}$	μ_r	ϵ_r	η	Γ_{PEC}	Γ_{PMC}
Form. $\mathbf{H}$	$\mathbf{H}$	ϵ_r	μ_r	$\frac{1}{\eta}$	Γ_{PMC}	Γ_{PEC}

$$\boldsymbol{\nabla} \times \frac{1}{\mathbf{f_r}} \boldsymbol{\nabla} \times \mathbf{V} - k_0^2 \boldsymbol{g_r} \mathbf{V} = \mathbf{O} \tag{10}$$

where $\mathbf{O}$ stands for term associated to the interior sources of the domain (electric and magnetic currents).

Boundary conditions considered are the following:

$$\hat{\mathbf{n}} \times \mathbf{V} = 0, \text{at } \Gamma_D \tag{11}$$

$$\hat{\mathbf{n}} \times \frac{1}{f_r} \boldsymbol{\nabla} \times \mathbf{V} = 0, \text{at } \Gamma_N \tag{12}$$

$$\hat{\mathbf{n}} \times \left(\frac{1}{f_r} \boldsymbol{\nabla} \times \mathbf{V} \right) + \gamma \hat{\mathbf{n}} \times \hat{\mathbf{n}} \times \mathbf{V} = \boldsymbol{\Psi}, \text{at } \Gamma_C \tag{13}$$

where $\boldsymbol{\Psi}$ represents the excitation from the exterior of the domain (either waveports or exterior boundary for open region problems). Symbol γ denotes the appropriate propagation constant.

The variational formulation associated is obtained by multiplying (10) with a test function $\boldsymbol{F}$:

Find $\mathbf{V} \in \mathbf{W}$ such that

$$c_1(\mathbf{F}, \mathbf{V}) - k_o^2 \, c_2(\mathbf{F}, \mathbf{V}) + \gamma \, c_3(\mathbf{F}, \mathbf{V}) = l(\mathbf{F}), \quad \forall \mathbf{F} \in \mathbf{W} \tag{14}$$

where bilinear forms $c_1(\mathbf{F}, \mathbf{V})$, $c_2(\mathbf{F}, \mathbf{V})$ and $c_3(\mathbf{F}, \mathbf{V})$ are given by:

$$\begin{aligned} c_1(\mathbf{F}, \mathbf{V}) &= \int_\Omega (\boldsymbol{\nabla} \times \mathbf{F}) \cdot (\frac{1}{f_r} \boldsymbol{\nabla} \times \mathbf{V}) \, d\Omega \\ c_2(\mathbf{F}, \mathbf{V}) &= \int_\Omega \mathbf{F} \cdot g_r \mathbf{V} \, d\Omega \\ c_3(\mathbf{F}, \mathbf{V}) &= \int_{\Gamma_{\text{C}}} (\hat{\mathbf{n}} \times \mathbf{F}) \cdot (\hat{\mathbf{n}} \times \mathbf{V}) \, d\Gamma_{\text{C}} \end{aligned} \tag{15}$$

and linear form $l(\mathbf{F})$ by

$$l(\mathbf{F}) = \int_\Omega (\mathbf{F} \cdot \mathbf{O}) \, d\Omega \tag{16}$$

where

$$\mathbf{W} := \{ \mathbf{A} \in \mathbf{H}(\text{curl}, \Omega), \; \hat{\mathbf{n}} \times \mathbf{A} = 0 \text{ on } \Gamma_D \} \tag{17}$$

and Ω is the problem domain.

Thus, MMS is used in our case by choosing a given vector function $\mathbf{V}$ (denoted as $\mathbf{V}_{\text{MMS}}$) and computing $\mathbf{O}$ in (10) and $\boldsymbol{\Psi}$ in (13). These computed functions $\mathbf{O}$ and $\boldsymbol{\Psi}$ are introduced as data to the FEM code (through variational formulation (15)). The numerical approximated solution given by FEM code is obtained (denoted by $\mathbf{V}_{\text{FEM}}$). The energy error between $\mathbf{V}_{\text{MMS}}$ and $\mathbf{V}_{\text{FEM}}$ is computed, namely error in the field itself and its

TABLE IV: Relative errors for different mesh sizes of a cube using a polynomial as manufactured solution.

Elements	Unknowns	ξ_{REL}	$(\nabla \times \xi)_{\text{REL}}$
128	2232	1.872E-13	1.017E-14
260	4330	2.918E-13	1.204E-14
2080	31820	1.053E-12	2.338E-14

curl separately:

$$\varsigma = \frac{\| c_2 \left((\mathbf{V}_{\text{FEM}} - \mathbf{V}_{\text{MMS}}), (\mathbf{V}_{\text{FEM}} - \mathbf{V}_{\text{MMS}})^* \right) \|_2}{\| c_2 \left(\mathbf{V}_{\text{MMS}}, \mathbf{V}^*_{\text{MMS}} \right) \|_2} \tag{18}$$

$$\varsigma_{\text{curl}} = \frac{\| c_1 \left((\mathbf{V}_{\text{FEM}} - \mathbf{V}_{\text{MMS}}), (\mathbf{V}_{\text{FEM}} - \mathbf{V}_{\text{MMS}})^* \right) \|_2}{\| c_1 \left(\mathbf{V}_{\text{MMS}}, \mathbf{V}^*_{\text{MMS}} \right) \|_2} \tag{19}$$

In the following, results corresponding to the application of MMS on a cube shaped domain are shown. Different finite element meshes have been used in the experiment. Several types of manufactured solutions have also been used in the analysis. Polynomial manufactured solutions belonging to the vector space of second order basis functions described in (3) were tried first. Results corresponding to manufactured solution $\mathbf{V}_{\text{MMS}} = (xyz^2, -xz^2, xyz)$, are shown here. Analogous results are obtained with other elements of space given in (3) and thus, they are omitted. It is important to note that the error expected in these cases is numerically zero, i.e. close to the machine precision. Results of the relative error of the field, and its curl, with different meshes are shown in Table IV. It is observed that errors are close to machine precision (double precision is used in the code). As expected, a slight increment in the error is detected with finer mesh discretizations due to the accumulation of numerical noise with the number of floating point operations. It may visually observed in the **Figure** 5 that the numerical error is homogeneously distributed and there are not *hot spots*, or isolated points with error orders of magnitude greater.

A convergence analysis has been performed by using MMS with a complex exponential function as manufactured solution; namely

$$\mathbf{V}_{\text{MMS}} = \mathbf{V}_{\text{pol}} e^{-jk_0(\hat{\mathbf{k}}_p \cdot \boldsymbol{r})} \tag{20}$$

where $\mathbf{V}_{\text{pol}}$ is the polarization vector, $\hat{\mathbf{k}}_p$, the unit propagation vector and $\mathbf{r}$ the position vector.

As the complex exponential function does not belong to the space of basis functions, the error expected is not numerically zero, but it should converge to zero when the number of prisms of the mesh is increased. Specifically, for smooth functions (as it is the case of the exponential function) the behavior of the error in the asymptotic regime predicted by the theory (see e.g., [2], [36]) is error $= C\, h^p$, where h denotes the diameter of the element. Thus, a plot of the error with $1/h$ in logarithmic scale should look like a straight line with a negative slope equal to 2 ($p = 2$ in our case). Numerical results of the convergence study are shown in Figure 4. Two polarizations, $\mathbf{V}_{\text{pol}} = \hat{\boldsymbol{\theta}}$ and $\mathbf{V}_{\text{pol}} = \hat{\boldsymbol{\phi}}$, and different angles of incidence, have been considered. In all cases, it is observed that the obtained error follows almost perfect straight lines. Different error levels are obtained depending on the

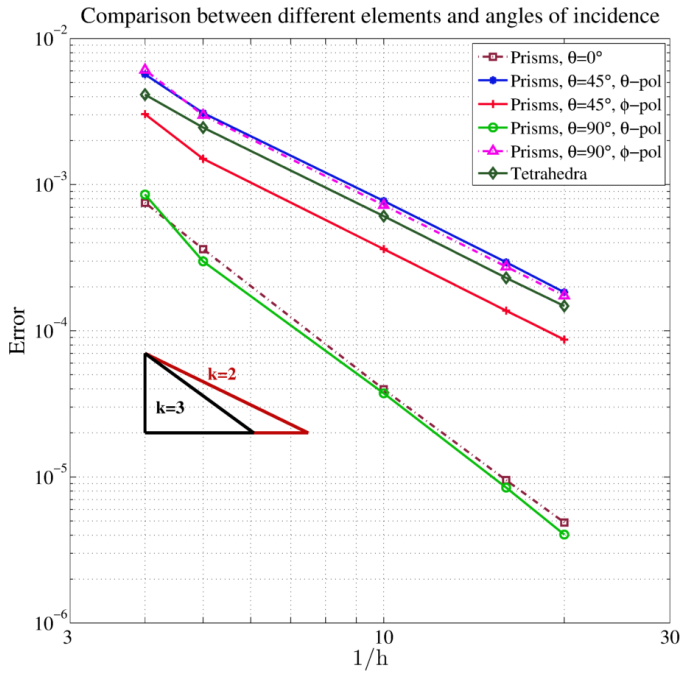

Fig. 4: **Convergence rate of the error over a cube using a complex exponential as manufactured solution with different incidence angles, different polarizations and different elements with a frequency of 100 MHz.**

angle of incidence with respect to the prisms and on the polarization. Furthermore, in some specific cases the slope is even greater (**in absolute value**) than 2. Specifically, a sort of superconvergence behaviour (slope equal to 3) is observed for angle of incidence $\theta = 0°$ independently of the polarization. The same behaviour is obtained for $\theta = 90°$ only with θ-polarization. By departing a few degrees from those specific angles the superconvergence behavior is lost and the slope is reverted to 2. For comparison purposes the convergence of the error with second order tetrahedra of the same family [2], [31] is also shown in the figure. Note that the error observed using tetrahedra is the same independently of the angle of incidence and polarization. **Text has been omitted here. Text omitted included comments about the lack of symmetric/isotropiy of the prism in contrast with the tetrahedron.**

Results above are enough to verify the correctness of the basis functions and its implementation as manufactured solutions belonging the space of polynomials $\mathcal{P}_2^{\text{prism}}$ are reproduced with (numerically) zero error. Also, the excellent agreement of the obtained rates of convergence of the error with those predicted by FEM theory for regular solutions is also a proof of verification of the variational formulation, mesh generation, and so on. Nevertheless, the analysis of a number of cavity problems were also perfomed for further validation purposes. Variational formulation described by expressions (14)–(17) was converted into a generalized eigenvalue problem setup with k_o^2 as eigenvalue by simply removing bilinear form $c_3(\mathbf{F}, \mathbf{V})$ and linear form $l(\mathbf{F})$. Results of one homogenous cavity and one inhomogenous cavity used before in the literature

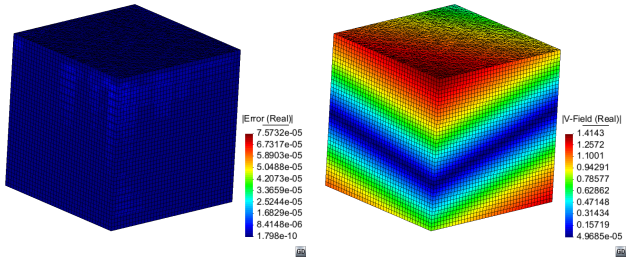

(a) Error between analytic and code solution, ς

(b) Code solution

Fig. 5: **Illustration of MMS verification. On (a) it is shown the error ς corresponding to a polynomial manufactured solution $\mathbf{V}_{\mathbf{MMS}} = (xyz^2, -xz^2, xyz)$, while on (b) it is shown $|Re(\mathbf{V}_{\mathbf{FEM}})|$ corresponding to an exponential manufactured solution (expression 20).**

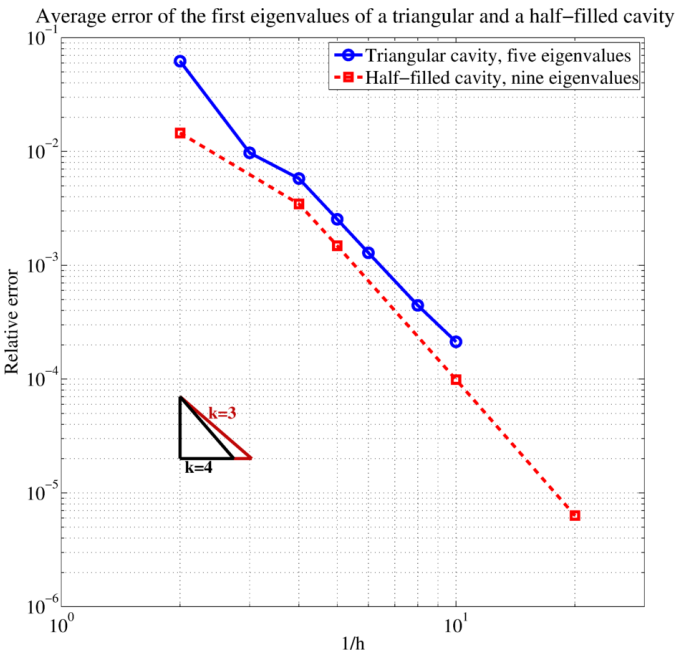

Fig. 6: **Convergence rate of the average error of the first eigenvalues of metallic cavities. The triangular prism cavity has an equilateral triangular base and the height of the cavity is equal to the length of the triangular side (see [16]). The half filled cavity has been widely used in the literature (e.g., [37]). This cavity is of rectangular shape and dimensions $(1, 0.1, 1)$ being half filled with dielectric of $\epsilon_r = 2$ in the upper half part of the third dimension.**

as benchmark structures have been selected. Figure 6 shows the convergence rate of the average error in the computation of the first eigenvalues of a metallic prism empty cavity and a non-homogeneous cavity; specifically of a metallic cavity half-filled with dielectric. In both cases, obtained rate of convergence is very close to the expected theoretical rate of h^{2p}, [2], i.e., h^4 in our case.

As conclusion from above, it can be stated the correctness of the basis functions and their implementation has been verified.

In the following, results showing the robustness of the prism, in the sense of the condition number of the FEM matrices, with respect to distortions in its shape are explained. **Comparison with the basis functions provided in [16] and a version inspired in [27] are included. Second order version of the basis functions of [16] were implemented in code and checked to span exactly the same space than the ones of this paper, i.e., precisely Nédélec mixed order space for the prism [21] described in expression (3). Basis functions of a second mixed-order prism inspired in the spectral element proposed in [27] have also been coded and checked that they span the same space of functions that the other two. Lagrange interpolatory polynomials were used instead of polynomials based on Gauss-Legendre-Lobatto integration points as shown in [27]. Specifically, the basis coded are the following:**

$$\begin{aligned}
L_m L_l^2 \mathbf{W}_{ij};\ i,j=1,2,3; j>i; m=i,j; l=4,5\\
L_i^2 L_l \nabla L_l;\ i=1,2,3; l=4,5\\
L_k L_l^2 \mathbf{W}_{ij};\ i,j,k=1,2,3; j>i; k\neq i,j; l=4,5\\
L_m L_l L_{l+1} \mathbf{W}_{ij};\ i,j=1,2,3; j>i; m=i,j; l=4\\
L_i L_j L_l \nabla L_l;\ i,j=1,2,3; j>i; l=4,5\\
L_k L_l L_{l+1} \mathbf{W}_{ij};\ i,j,k=1,2,3; j>i; k\neq i,j; l=4
\end{aligned} \tag{21}$$

where set (L_1, L_2, L_3) corresponds to the affine coordinates for the triangle and (L_4, L_5) are the affine coordinates for the segment (connecting triangular faces). Symbol $\mathbf{W}_{ij}$ stands for the Whitney function $L_i \nabla L_j - L_j \nabla L_i$. The third subset of basis are face functions associated to the upper and bottom triangular faces. For each face, only two of the three possible basis must be selected. The sixth subset of basis are interior functions and, analogously, only two basis functions must be chosen.

Thus, three representative different sets of basis functions for the prism are considered in the comparison. Second order basis functions of [16] (denoted there as $p = 1$) and those of (21) are based on a explicit construction using Whitney functions multiplied by appropriate polynomials. In the case of [16] polynomials are constructed based on fully interpolatory properties on a number of points on the whole prism in general. On the other hand, basis functions proposed in this paper are not interpolatory in the above sense as it was mentioned in Section II-D. The case of functions described in (21) is somehow intermediate. Basis functions are naturally associated to edges, faces and interior, and interpolatory polynomials used on the explicit construction of the basis are defined in terms of points but only on the corresponding entity (edges, faces, or interior) but not over the whole prism.

The condition number is defined as the ratio of the maximum and minimum eigenvalue of the matrices corresponding to the inner products of the vector basis functions in a finite element and of their curls, i.e., element mass matrix $[M]$ and stiffness matrix $[K]$, as they are typically known among FEM

practitioners:

$$M_{ij} = c_2(\boldsymbol{N}_i, \boldsymbol{N}_j) \quad (22)$$

$$K_{ij} = c_1(\boldsymbol{N}_i, \boldsymbol{N}_j) \quad (23)$$

It has to be noted that numerically null eigenvalues of the stiffness matrix have been discarded.

In the author's experience a straight comparison between sets of basis functions in terms of the condition number of FEM matrices can be misleading if normalization is not taken into account. Then, the condition number actually computed corresponds to the preconditioned matrices $[M^p]$ and $[K^p]$

$$[M^p] = [D]^{-1}[M][D]^{-1} \quad (24)$$

$$[K^p] = [D]^{-1}[K][D]^{-1} \quad (25)$$

where $[D]$ is a diagonal matrix with $D_{ii} = \sqrt{M_{ii}}$, i.e., by normalizing the basis functions.

In the case of functions of [16], the specific normalization factors proposed by their authors are used prior to the pre-scaling using $[D]$. It is important to note that in all cases, the condition number of the preconditioned matrices $[M^p]$ and $[K^p]$ is always better than the original ones for the three sets of basis functions compared.

Two different types of deformation of the reference element have been implemented**: "triangle deformation" and "rectangle deformation". The triangle deformation case** is made by stretching out the triangular bases of the prisms (the quadrilateral faces are kept rectangular). In the **rectangle deformation case**, the prism is generated by extrusion in an inclined direction (non orthogonal to triangle base). Thus, rectangular faces of the reference element are transformed into parallelograms more and more stretched out. Specifically, results shown correspond to the coordinates for the prism vertices included in Table IX.

Condition numbers are shown in Tables V, VI, VII and VIII. The Tables V and VI show the conditions numbers for the triangle deformation for the mass and stiffness matrices, respectively. Three cases of the *vc* version of the basis function proposed in this paper (see Section II-E) are considered depending if the directions $\widehat{\alpha}$ and $\widehat{\beta}$ of vectors q are chosen parallel to edges 1-2, 2-3 or 3-1 of the triangle faces (same q are selected on the upper and bottom triangular faces of the prism). Only one case of the *vq* version of the basis function proposed in this paper is shown. In the *vq* strategy directions $\widehat{\alpha}$ and $\widehat{\beta}$ are chosen orthogonal and it is observed that the condition numbers resulting of different choices of orthogonal pairs of vectors q provide nearly the same condition number. It is clearly observed that *vq* strategy always returns optimum condition numbers compared with the *vc* versions. Note that in the particular case of the triangle deformation considered here there is one *vc* combination that corresponds to orthogonal directions and, hence, it provides identical condition numbers to those of the *vq* strategy. In the case of specially distorted elements, the difference in conditioning between the best *vc* combination and the *vq* strategy can be considerable.

TABLE V: Condition number of mass matrices for different cases of prisms (triangle deformation).

	Reference prism	Triangle deformation		
		$\kappa = 4$	$\kappa = 8$	$\kappa = 16$
Version	$[M^p]$	$[M^p]$	$[M^p]$	$[M^p]$
vc,(1-2)	81	1587	18826	276385
vc,(2-3)	81	217	738	2827
vc,(3-1)	71	215	737	2825
vq	72	215	737	2826
Graglia,(2-3)+(1-2)	33	173	638	2497
Graglia,(3-1)+(1-2)	37	174	639	2498
Tobon(3-1)	301	1020	3967	15871
Tobon(2-3)	171	1021	3967	15871
Tobon(1-2)	171	842	3468	14046

As illustration consider the condition numbers obtained for the mass matrix with the *vc* case labeled as 1-2.

In the case of Tables VII and VIII, and because of the particular case of rectangle deformation considered here in which the rectangular faces are parallelograms, only one *vc* case is possible. Again, with the *vq* strategy orthogonal directions $\widehat{\alpha}$ and $\widehat{\beta}$ are selected. Similar statements to those just made about the impact of triangle deformation in the condition number hold here. However, as it is observed in the tables, the effect of the orthogonality of the vq vectors has a lower impact in the case of rectangle deformation, at least, for the type of deformation considered. [OPCIONAL: The difference in behavior between triangle and rectangle deformations is again a consequence of the tensor product structure of the prism that somehow hybridizes tetrahedron and hexahedron types of behavior.]

When comparing the basis functions proposed in this paper with the others considered in the comparison the following observations can be made. Note that different combinations of basis functions of [16] associated to triangular faces have been considered. And analogously happen with those of (21). Basis functions of [16] provide the best conditioning in all cases. Basis functions proposed here are competitive with respect to the one of [16] in terms of condition number. Both sets of basis functions provide same order of magnitude for the mass and stiffness matrices. That does not happen with basis functions of (21) in which the condition number of the mass matrix for both types of deformation is roughly one order of magnitude higher than with the other sets of basis functions.

It can be observed the condition number varies with the aspect ratio of the elements, being larger in the cases in which the aspect ratio is larger, as expected. Two versions of the assembly procedure are presented in the tables. In the case denoted by *vc* (see Section II-E) directions $\widehat{\alpha}$ and $\widehat{\beta}$ are chosen parallel to the edges that define the face in which they are contained. In the case denoted here by *vq*, directions $\widehat{\alpha}$ and $\widehat{\beta}$ are chosen orthogonal. It is observed that the effect of the deformation of the prism shape in the condition number is different when it affects to the triangular base than when it deforms the rectangular faces. This is again a consequence

TABLE VI: Condition number of stiffness matrices for different cases of prisms (triangle deformation).

	Reference prism	Triangle deformation		
		$\kappa = 4$	$\kappa = 8$	$\kappa = 16$
Version	$[K^p]$	$[K^p]$	$[K^p]$	$[K^p]$
vc,(1-2)	37	210	791	3096
vc,(2-3)	37	199	733	2856
vc,(3-1)	38	197	732	2854
vq	37	197	732	2854
Graglia,(2-3)+(1-2)	16	102	394	1555
Graglia,(3-1)+(1-2)	19	104	394	1551
Tobon(3-1)	24	108	417	1659
Tobon(2-3)	20	109	418	1659
Tobon(1-2)	20	101	398	1588

TABLE VII: Condition number of mass matrices for different cases of prisms (rectangle deformation).

	Reference prism	Rectangle deformation		
		$\varepsilon = 2$	$\varepsilon = 4$	$\varepsilon = 8$
Version	$[M^p]$	$[M^p]$	$[M^p]$	$[M^p]$
vc	72	3107	12270	48926
vq	72	2187	8435	33432
Graglia	37	1484	5889	23509
Tobon	301	5967	23559	93928

TABLE VIII: Condition number of stiffness matrices for different cases of prisms (rectangle deformation).

	Reference prism	Rectangle deformation		
		$\varepsilon = 2$	$\varepsilon = 4$	$\varepsilon = 8$
Version	$[K^p]$	$[K^p]$	$[K^p]$	$[K^p]$
vc	37	2566	10205	40765
vq	37	2066	8171	32599
Graglia	19	1067	4279	17131
Tobon	24	1209	4226	16923

TABLE IX: Coordinates of the prisms used in the analysis of the condition number.

Triangle deformation		Rectangle deformation	
Vertex	Coordinates	Vertex	Coordinates
$\boldsymbol{r}_1$	$(0,0,0)$	$\boldsymbol{r}_1$	$(0,0,0)$
$\boldsymbol{r}_2$	$(\varepsilon,0,0)$	$\boldsymbol{r}_2$	$(1,0,0)$
$\boldsymbol{r}_3$	$(0,1,0)$	$\boldsymbol{r}_3$	$(0,1,0)$
$\boldsymbol{r}_4$	$(0,0,1)$	$\boldsymbol{r}_4$	$(2,2,1/\kappa)$
$\boldsymbol{r}_5$	$(\varepsilon,0,1)$	$\boldsymbol{r}_5$	$(3,2,1/\kappa)$
$\boldsymbol{r}_6$	$(0,1,1)$	$\boldsymbol{r}_6$	$(2,3,1/\kappa)$

of the tensor product structure of the prism. It can also be observed that the condition number is always lower with the *vq* strategy. This is specially significative for the mass matrix with "triangle deformation". The *vq* strategy obtains the best results for both matrices $[M^p]$ and $[K^p]$; up to an order of magnitude better in the case of triangle deformation and the mass matrix. It is concluded that the *vq* strategy works better with irregular meshings since the elements are more deformed, while the *vc* strategy obtains similar results with regular elements. On the other hand, *vc* strategy has advantages as it was explained in Section II-E.

IV. Conclusions

Basis functions of the second order Nédélec mixed order curl-conforming prism have been obtained following a sound mathematical approach. A systematic method to discretize Nédélec functionals acting as degrees of freedom has been shown. Correctness of the so obtained basis functions have been thoroughly verified. Several strategies of assembly and its impact in the condition number of the resulting matrices in distorted meshes have been presented. **Comparison with other representative sets of basis functions for prisms has been included.**

References

[1] J. C. Nédélec, "Mixed finite elements in R^3," *Numerische Mathematik*, vol. 35, pp. 315–341, 1980.

[2] M. Salazar-Palma, T. K. Sarkar, L. E. García-Castillo, T. Roy, and A. R. Djordjevic, *Iterative and Self-Adaptive Finite-Elements in Electromagnetic Modeling*. Norwood, MA: Artech House Publishers, Inc., 1998.

[3] J. P. Webb, "Hierarchal vector basis functions of arbitrary order for triangular and tetrahedral finite elements," *IEEE Transactions on Antennas and Propagation*, vol. 47, no. 8, pp. 1244–1253, Aug. 1999.

[4] T. V. Yioultsis and T. B. Tsiboukis, "Convergence-optimized, higher order vector finite elements for microwave simulations," *IEEE Microwave and Wireless Components Letters*, vol. 11, no. 10, pp. 419–421, Oct. 2001.

[5] M. M. Ilíc and B. M. Notaroš, "Higher order hierarchical curved hexaedral vector finite elements for electromagnetic modeling," *IEEE Transactions on Microwave Theory and Techniques*, vol. 51, no. 3, pp. 1026–1033, Mar. 2003.

[6] Z. Ren and N. Ida, "Solving 3D eddy current problems using second order nodal and edge elements," *IEEE Transactions on Magnetics*, vol. 36, no. 4, pp. 746–749, Jul. 2000.

[7] D. K. Sun, J. F. Lee, and Z. Csendes, "Construction of nearly orthogonal Nedelec bases for rapid convergence with multilevel preconditioned solvers," *SIAM Journal of Scientific Computing*, vol. 23, no. 4, pp. 1053–1076, 2003.

[8] L. F. Demkowicz, *Encyclopedia of Computational Mechanics*. John Wiley & Sons, Inc., 2004, ch. "Finite Element Methods for Maxwell Equations".

[9] L. F. Demkowicz, P. Monk, L. Vardapetyan, and W. Rachowicz, "De Rham diagram for *hp* finite element spaces," *Computer and Mathematics with Applications*, vol. 39, no. 7-8, pp. 29–38, 2000.

[10] L. E. García-Castillo and M. Salazar-Palma, "Second-order Nédélec tetrahedral element for computational electromagnetics," *International Journal of Numerical Modelling: Electronic Networks, Devices and Fields (John Wiley & Sons, Inc.)*, vol. 13, no. 2-3, pp. 261–287, March-June 2000.

[11] L. E. García-Castillo, A. J. Ruiz-Genovés, I. Gómez-Revuelto, M. Salazar-Palma, and T. K. Sarkar, "Third-order Nédélec curl-conforming finite element," *IEEE Transactions on Magnetics*, vol. 38, no. 5, pp. 2370–2372, Sep. 2002.

[12] D. Garcia-Donoro, I. Martinez-Fernandez, L. E. Garcia-Castillo, and M. Salazar-Palma, "HOFEM: A higher order finite element method electromagnetic simulator," in *12th International Workshop on Finite Elements for Microwave Engineering*, Mount Qingcheng, Chendu, China, May 2014.

[13] K. Hirayama, M. S. Alam, Y. Hayashi, and M. Koshiba, "Vector finite element method with mixed-interpolation-type triangular-prism element for waveguide discontinuities," *IEEE Transactions on Microwave Theory and Techniques*, vol. 42, no. 12, pp. 2311–2316, Dec. 1994.

[14] Z. Sacks and J.-F. Lee, "A finite-element time-domain method using prism elements for microwaves cavities," *IEEE Transactions on Electromagnetic Compatibility*, vol. 37, no. 4, pp. 519–527, Nov. 1995.

[15] T. Ozdemyr and J. L. Volakis, "Triangular prisms for edge-based vector finite element analysis of conformal antennas," *IEEE Transactions on Antennas and Propagation*, vol. 45, no. 5, pp. 788–797, May 1997.

[16] R. D. Graglia, D. R. Wilton, and A. F. Peterson, "Higher order interpolatory vector bases on prism elements," *IEEE Transactions on Antennas and Propagation*, vol. 46, no. 3, pp. 442–450, Mar. 1998.

[17] ——, "Higher order interpolatory vector bases for computational electromagnetics," *IEEE Transactions on Antennas and Propagation*, vol. 45, no. 3, pp. 329–342, Mar. 1997.

[18] D. I. Karatzidis, T. V. Yioultsis, and T. B. Tsiboukis, "Efficient analysis of planar microwave circuits with mixed-order prism vector finite macroelements," *International Journal of Numerical Modelling: Electronic Networks, Devices and Fields (John Wiley & Sons, Inc.)*, vol. 21, no. 6, pp. 475–492, Nov. 2008.

[19] ——, "General multiple order prism vector finite macroelements for planar microwave circuits and EBGs," *IEEE Transactions on Magnetics*, vol. 45, no. 3, pp. 1056–1059, Mar. 2009.

[20] T. V. Yioultsis and T. B. Tsiboukis, "Multiparametric vector finite elements: a systematic approach to the construction of three-dimensional, higher order, tangential vector shape functions," *IEEE Transactions on Magnetics*, vol. 32, no. 3, pp. 1389–1392, May 1996.

[21] J. C. Nédélec, "A new family of mixed finite elements in $\Re^3$," *Numerische Mathematik*, vol. 50, pp. 57–81, 1986.

[22] D. Chen and D. Jiao, "Time-domain orthogonal finite-element reduction-recovery method for electromagnetics-based analysis of large-scale integrated circuit and package problems," *IEEE Transactions on Computer Aided Design Integrated Circuits*, vol. 28, no. 8, pp. 1138–1149, Aug. 2009.

[23] J. Lee, D. Chen, V. Balakrishnan, C.-K. Koh, and D. Jiao, "A quadratic eigenvalue solver of linear complexity for 3-D electromagnetics-based analysis of large-scale integrated circuits," *IEEE Transactions on Computer Aided Design Integrated Circuits*, vol. 31, no. 3, pp. 380–390, Mar. 2012.

[24] D. A. White, "Orthogonal vector basis functions for time domain finite element solution of the vector wave equation," *IEEE Transactions on Magnetics*, vol. 35, no. 3, pp. 1458–1461, May 1999.

[34] D. Garcia-Doñoro, L. E. García-Castillo, and S. W. Ting, "Verification process of finite-element method code for electromagnetics: Using the

[25] D. Jiao, M. Lu, E. Michielssen, and J. M. Jin, "A fast time-domain finite element-boundary integral method for electomagnetic analysis," *IEEE Transactions on Antennas and Propagation*, vol. 49, no. 10, pp. 1453–1461, Oct. 2001.

[26] D. Jiao and J. M. Jin, "Three-dimensional orthogonal vector basis functions for time-domain finite element solution of vector wave equations," *IEEE Transactions on Antennas and Propagation*, vol. 51, no. 1, pp. 59–66, Jan. 2003.

[27] L. E. Tobon, Q. Ren, and Q. H. Liu, "Spectral-prism element for multi-scale layered package-chip co-simulations using the discontinuous galerkin time-domain method," *Electromagnetics*, vol. 34, pp. 270–285, 2014, prisma con funciones spectrales en la direccion z.

[28] S. Zaglmayr, "Higher order finite element methods for electromagnetic field computation," Ph.D. dissertation, Johannes Kepler Universit at Linz, Jul. 2006.

[29] P. G. Ciarlet, *The Finite Element Methods for Elliptic Problems*. New York: North Holland, 1994.

[30] J. N. Reddy, *An Introduction to the Finite Element Method.* McGraw-Hill, 1984, 1993.

[31] A. J. Ruiz-Genovés, L. E. García-Castillo, M. Salazar-Palma, and T. K. Sarkar, "A mixed-order curl-conforming family of simplex finite-elements for electromagnetic modeling," in *International Conference on Electromagnetics in Advanced Applications (ICEAA01)*, Torino (Italia), Sep. 2001, pp. 873–876, Invited paper.

[32] J. Gopalakrishan, L. E. García-Castillo, and L. F. Demkowicz, "Nédélec spaces in affine coordinates," *Computer & Mathematics with Applications*, vol. 49, no. 7/8, pp. 1285–1294, May-June 2005, doi:10.1016/j.camwa.2004.02.012. Available as TICAM REPORT 03/48, Nov-2003.

[33] P. J. Roache, *Verification and Validation in Computational Science and Engineering*. Alburquerque: Hermosa Publishers, 1998.
method of manufactured solutions," *IEEE Antennas and Propagation Magazine*, vol. 7, no. 2, pp. 28–38, Apr. 2016.

[35] D. García Donoro, "A new software suite for electromagnetics," Jul. 2014, tesis Doctoral. Universidad Carlos III de Madrid. Calificación: Sobresaliente *cum laude*.

[36] J. T. Oden and J. N. Reddy, *An Introduction to the Mathematical Theory of Finite Elements*, ser. Pure and Applied Mathematics. A Wiley-Interscience Series of Texts, Monographs and Tracts. John Wiley & Sons, Inc., 1976.

[37] A. Chatterjee, J. M. Jin, and J. L. Volakis, "Computation of cavity resonances using edge-based finite elements," *IEEE Transactions on Microwave Theory and Techniques*, vol. 40, no. 11, pp. 2106–2108, Nov. 1992.